NUMERICAL ANALYSIS OF SCATTERED POWER FROM A LAYER OF RANDOM MEDIUM CONTAINING MANY PARTICLES OF HIGH DIELECTRIC CONSTANT – APPLICATION TO THE DETECTION OF A WATER CONTENT OF SOIL –

T. Matsuoka and M. Tateiba

Department of Computer Science and Communication Engineering
Graduate School of Information Science and Electrical Engineering
Kyushu University
6-10-1 Hakozaki, Higashi-ku, Fukuoka 812-8581, Japan

Abstract—This paper shows the scattering cross sections of a random medium which is a simple model of moist soil by analyzing a dense medium radiative transfer equation (DMRT). The parameters in the DMRT, the extinction rate and the scattering coefficient, are calculated by a multiple scattering method called our method in this paper. Our method is valid for particles with high dielectric constant like water drops. Characteristics of the scattering cross section are made clear by changing the fractional volume of water and the incident angle, polarization of incident waves. We discuss the possibility of detection of a water content in this approach by using the characteristics of the scattering cross section.

1. INTRODUCTION

Remote sensing for earth terrain such as snow, ice and soil has attracted attention for widely measuring earth environment. The detection of a water content of soil is one of important problems in civil and agricultural engineering, and has therefore been studied in active and passive remote sensing approaches [1, 2]. Microwave remote sensing seems to be a promising one because the properties of moist soil for microwave are sensitive to a water content [3].

Moist soil is composed of air, soil particles, bound water and free water [3, 4] and may be regarded as a dense random medium from a theoretical point of view. Theoretical approaches have not been made a lot of progress in the remote sensing because the particles of high dielectric constant such as water drops make it difficult to take account multiple scattering effects into the analysis of interaction of waves with random media. One of the authors presented recently a multiple scattering method which is applicable to particles of high dielectric constant [5, 6]. By using the method, we now investigate the characteristics of scattered power by a random medium when the distribution of particles containing water changes from sparsely to densely.

Radiative transfer equations have been used to analyze the transport of wave intensity in a random medium. A conventional radiative transfer equation (CRT) based on the transport of energy through the medium becomes invalid for a dense random medium such a moist soil. Another radiative transfer equation called dense medium radiative transfer equation (DMRT) has been derived from a wave equation by applying the Quasi Crystalline Approximation with Coherent Potential (QCA-CP) and the ladder approximation to the first and second moments of waves [7]. Under these approximations, the random medium can be regarded as a homogeneous medium with the effective dielectric constant evaluated by QCA-CP in Rayleigh scattering region; and the effective dielectric constant is closely related to the scattering coefficient and the extinction rate in the DMRT. It has been, however, shown that QCA-CP becomes invalid for a random medium with particles of high dielectric constant [5, 6].

Another method for evaluating the effective dielectric constant has been presented by one of the authors [8, 9], which is called "our method" in this paper. It has been shown that our method is physically valid even for particles of high dielectric constant like water drops, where other methods including QCA-CP become invalid [5, 6]. Numerical comparison of scattered power between four methods including QCA-CP and our method [10] has shown that it is highly important to evaluate the effective dielectric constant precisely for calculating the scattering cross section of a random medium by using a radiative transfer equation.

For developing a method for detecting a water content of soil by active remote sensing, this paper deals with a three layer model composed of air, moist soil layer and bottom layer. The moist soil layer is assumed to be a random medium where identical spherical particles are embedded in a homogeneous background medium. We consider two types of the particles: water drops and soil particles coated with water. A radiative transfer equation with the parameters evaluated by our method are used in the random medium to calculate the scattering cross section of the moist soil layer. The calculation makes numerically clear the characteristics of scattering cross section of the layer by changing the fractional volume of water and the incident angle, polarization of incident waves. From the numerical results, we discuss the possibility of detection of the water content in this approach by considering the effects of layer thickness and bottom layer. It should be noted that we do not need to take backscattering enhancement into account because the scattering effect of water drops is small as will be mentioned in Subsection 2.2.

2. FORMULATION

Let us consider a layer of random medium of $\varepsilon_g \varepsilon_0$ and thickness d (region 1) where identical spheres of radial dielectric constant profile $\varepsilon_1(r)\varepsilon_0$ and radius a are embedded. The layer is over a semi-infinite layer of $\varepsilon_2 \varepsilon_0$ (region 2) and under air ε_0 (region 0), as shown in Fig. 1. A polarized electromagnetic plane-wave is incident on region 1 from region 0 in the direction of $(\pi - \theta_{0i}, \phi_{0i})$. The specific intensity of the wave is assumed to satisfy a DMRT in region 1 and the boundary conditions at both boundaries between regions 0 and 1 and regions 1 and 2. The intensity in region 2 is easily estimated from that at the boundary because the region is a homogeneous medium. The extinction rate and the scattering coefficient in the DMRT are evaluated from the effective medium parameters in region 1 by using our method.
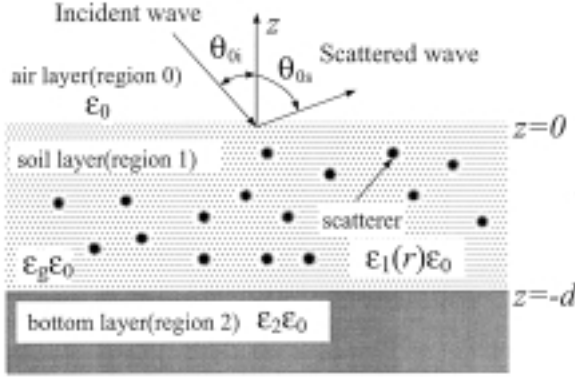
Figure 1. Geometry of the problem of wave scattering from a layer of discrete random medium.

2.1. Dense Medium Radiative Transfer Equation

The second moment of waves in a random medium generally obeys the Bethe-Salpeter equation. By applying the ladder approximation, the Bethe-Salpeter equation can be reduced to a DMRT. The DMRT in region 1 is written as, for $0 \le \theta \le \pi$,

$$\cos\theta \frac{\partial \boldsymbol{I}(\theta,\phi,z)}{\partial z} = -\kappa_{\mathrm{e}}\boldsymbol{I}(\theta,\phi,z) + \frac{\kappa_{\mathrm{s}}}{4\pi}\int_0^\pi \mathrm{d}\theta'$$
$$\cdot \sin\theta' \int_0^{2\pi}\mathrm{d}\phi' \mathbf{P}(\theta,\phi;\theta',\phi') \cdot \boldsymbol{I}(\theta',\phi',z), \qquad (1)$$

where $\boldsymbol{I}(\theta,\phi,z)$ is a 4×1 vector called the Stokes vector at z, given by

$$\boldsymbol{I}(\theta,\phi,z) = \begin{bmatrix} I_{\mathrm{v}} \\ I_{\mathrm{h}} \\ U \\ V \end{bmatrix} \qquad (2)$$

and $\mathbf{P}(\theta,\phi;\theta',\phi')$ is a 4×4 matrix, called phase matrix which describes the relation between the incident Stokes vector in the direction (θ',ϕ') and the scattered one in the direction (θ,ϕ), and is assumed the Rayleigh phase matrix [12] in this paper. Here κ_{e} and κ_{s} are the extinction rate and the scattering coefficient, respectively, and are closely related to the effective dielectric constant of a random medium $\varepsilon_{\mathrm{eff}}\varepsilon_0$; in other words, they depend on multiple scattering methods for estimating the $\varepsilon_{\mathrm{eff}}$.

On the other hand, the effective propagation constant $K(= K' + jK'')$ in the random medium can be expressed as

$$K^2 = k^2 \varepsilon_{\text{eff}} = k_{\text{g}}^2 + n_0 c \tag{3}$$

where k and k_{g}, respectively, are the wave number in free space and of the background medium, and n_0 denotes the distribution density of spheres. The $n_0 c$ shows the multiple scattering effects and is estimated by our method in this paper.

Let the mean distance between spherical particles be b, the fractional volume of particles be f and the relative contrast of each particle be $\varepsilon_{\text{d}}(r) = [\varepsilon_1(r) - \varepsilon_{\text{g}}]/\varepsilon_{\text{g}}$. According to our method [6, 8, 9], two forward scattering amplitudes F_1 and F_2 are introduced: they are, respectively, determined from the scattering of one particle with relative dielectric constant $[k_{\text{g}}^2 \varepsilon_{\text{d}}(r) + k_{\text{e}}^2]/k^2$ and $[k_{\text{g}}^2 \varepsilon_{\text{e}}(r) + k_{\text{e}}^2]/k^2$ in the medium of k_{e} for plane wave incidence. Here k_{e} and $\varepsilon_{\text{e}}(r)$ are expressed as the following equations [5]:

$$k_{\text{e}}^2 = k_{\text{g}}^2 \left[1 + \frac{4\pi}{b^3} \int_0^a \varepsilon_{\text{d}}(r_1) r_1^2 dr_1 \right] \tag{4}$$

$$\varepsilon_{\text{e}}(r) = \sqrt{\frac{2}{\pi}} \frac{1}{r\sigma} \exp\left[-\frac{r^2}{2\sigma^2} \right] \int_0^a \varepsilon_{\text{d}}(r_1) \exp\left[-\frac{r_1^2}{2\sigma^2} \right] \sinh\left[\frac{rr_1}{\sigma^2} \right] r_1 dr_1 \tag{5}$$

where σ^2 denotes the variance of random replacement of spherical particles from a uniformly ordered distribution. In this paper, we assume $\sigma/b = 1 - f$ for simplicity [6].

Consequently, the $n_0 c$ based on our method has been given as

$$n_0 c = k_{\text{e}}^2 - k_{\text{g}}^2 + \frac{4\pi}{b^3} \left\{ [F_1]_{\text{ria}} - [F_2]_{\text{ria}} \right\} + \frac{4\pi}{b^3} [F_1]_{\text{is}} \frac{(1-f)^4}{(1+2f)^2}. \tag{6}$$

Here the $[\ ]_{\text{ria}}$ and the $[\ ]_{\text{is}}$ are derived from a forward scattering amplitude of a particle F as follows. The F is composed of the real part F_{r} and the imaginary part $F_{\text{a}} + F_{\text{s}}$ where F_{a} and F_{s}, respectively, are produced by absorption and scattering; hence we define $[F]_{\text{ria}} = F_{\text{r}} + iF_{\text{a}}$ and $[F]_{\text{is}} = iF_{\text{s}}$. Then $[F]_{\text{is}}$ yields the coherence attenuation by multiple scattering. The equation (6) is also applicable to a random medium of lossless particles. For the lossless random medium, we have $F_{\text{a}} = 0$ and therefore the $[\ ]_{\text{ria}}$ and the $[\ ]_{\text{is}}$ correspond to "Re[ ]" and "i Im[ ]" described in [6], respectively.

In (1), κ_{e} and κ_{s}, respectively, are given as

$$\kappa_{\text{e}} = 2K'' \tag{7}$$

$$\kappa_{\text{s}} = \frac{n_0 |c|^2}{6\pi} \frac{(1-f)^4}{(1+2f)^2}. \tag{8}$$

The reflection and transmission angles at the boundaries are assumed to obey Snell's law for K' because $K' \gg K''$. The boundary conditions for the Stokes vector at $z = 0$ and $-d$ are as follows: for $0 \leq \theta \leq \pi/2$,

$$\begin{cases} \boldsymbol{I}(\pi - \theta, \phi, 0) = \mathbf{T}_{01}(\theta_0) \cdot \boldsymbol{I}_{0i}(\pi - \theta_0, \phi_0, 0) + \mathbf{R}_{10}(\theta) \cdot \boldsymbol{I}(\theta, \phi, 0) \\ \boldsymbol{I}(\theta, \phi, -d) = \mathbf{R}_{12}(\theta) \cdot \boldsymbol{I}(\pi - \theta, \phi, -d) \end{cases}$$
(9)

where $\boldsymbol{I}_{0i}(\pi - \theta_0, \phi_0, 0)$ is the Stokes vector of the incident plane-wave from region 0, and expressed as

$$\boldsymbol{I}_{0i}(\pi - \theta_0, \phi_0, 0) = \boldsymbol{I}_{0i} \frac{\delta(\theta_0 - \theta_{0i})\delta(\phi_0 - \phi_{0i})}{\sin \theta_0},$$
(10)

where $\delta(\cdot)$ is the Dirac delta function and $\boldsymbol{I}_{0i}(\pi - \theta_0, \phi_0, 0) = [I_{v0i}, I_{h0i}, U_{0i}, V_{0i}]^t$ where the superscript t denotes transposition. The reflection matrix $\mathbf{R}_{10}(\theta)$ relates the upward Stokes vector to downward one in region 1 at $z = 0$ for wave traveling from region 1 to 0. Similarly, $\mathbf{R}_{12}(\theta)$ is the reflection matrix for the Stokes vector at $z = -d$. $\mathbf{T}_{01}(\theta)$ denotes the transmission matrix which connects the downward Stokes vector in region 0 to that in region 1. The transmission and the reflection matrices for the Stokes vector are given in Appendix A. $\boldsymbol{I}(\theta, \phi, z)$ and $\boldsymbol{I}(\pi - \theta, \phi, z)$ denote the upward and downward propagating Stokes vectors in region 1, respectively.

The scattered Stokes vector $\boldsymbol{I}_{0s}(\theta_{0s}, \phi_{0s}, 0) = [I_{v0s}, I_{h0s}, U_{0s}, V_{0s}]^t$ in the direction (θ_{0s}, ϕ_{0s}) is expressed as

$$\boldsymbol{I}_{0s}(\theta_{0s}, \phi_{os}, 0) = \mathbf{T}_{10}(\theta_s) \cdot \boldsymbol{I}(\theta_s, \phi_s, 0),$$
(11)

where $\mathbf{T}_{10}(\theta_s)$ is the transmission matrix of the Stokes vector from region 1 to region 0. When we assume that an α-polarized wave intensity $I_{\alpha 0i}(\pi - \theta_{0i}, \phi_{0i}, 0)$ is incident on the random medium in the direction $(\pi - \theta_{0i}, \phi_{0i})$ and a β-polarized wave intensity $I_{\beta 0s}(\theta_{0s}, \phi_{0s}, 0)$ is scattered in the backward direction $(\theta_{0i}, \phi_{0i} + \pi)$, then the backscattering cross section $\sigma_{\beta\alpha}(\theta_{0i})$ is defined as

$$\sigma_{\beta\alpha}(\theta_{0i}) = 4\pi \frac{\cos \theta_{0i} I_{\beta 0s}(\theta_{0i}, \pi + \phi_{0i}, 0)}{I_{\alpha 0i}},$$
(12)

where $\alpha, \beta = $ vertically(v) or horizontally(h).

2.2. Numerical Solution of the DMRT

Water is lossy material in microwave region [4]. Therefore the scattering effect in the random medium becomes small, and we can

obtain an efficient solution of (1) by iteration. The radiative transfer equation and boundary conditions can be cast in an integral equation for $0 \le \theta \le \pi/2$ as follows.

$$
\begin{aligned}
\boldsymbol{I}(\theta, \phi, z) &= \mathrm{e}^{-\kappa_\mathrm{e} z \sec \theta} \mathbf{F}(\theta) \cdot \mathbf{R}_{12}(\theta) \cdot \mathbf{T}_{01}(\theta_0) \\
&\quad \cdot \boldsymbol{I}_{0\mathrm{i}}(\pi - \theta_0, \phi_0, 0) \mathrm{e}^{-2\kappa_\mathrm{e} d \sec \theta} \\
&\quad + \sec \theta \mathrm{e}^{-\kappa_\mathrm{e} z \sec \theta} \frac{\kappa_\mathrm{s}}{4\pi} \int_0^\pi \sin \theta' \mathrm{d}\theta' \int_0^{2\pi} \mathrm{d}\phi' \\
&\quad \cdot \Bigg[\int_{-d}^z \mathrm{d}z' \mathrm{e}^{\kappa_\mathrm{e} z' \sec \theta} \mathbf{P}(\theta, \phi; \theta', \phi') \cdot \boldsymbol{I}(\theta', \phi', z') \\
&\quad + \mathbf{F}(\theta) \cdot \mathbf{R}_{12}(\theta) \mathrm{e}^{-2\kappa_\mathrm{e} d \sec \theta} \int_{-d}^0 \mathrm{d}z' \mathrm{e}^{-\kappa_\mathrm{e} z' \sec \theta} \\
&\quad \cdot \mathbf{P}(\pi - \theta, \phi; \theta', \phi') \cdot \boldsymbol{I}(\theta', \phi', z') \\
&\quad + \mathbf{F}(\theta) \cdot \mathbf{R}_{12}(\theta) \cdot \mathbf{R}_{10}(\theta) \mathrm{e}^{-2\kappa_\mathrm{e} d \sec \theta} \\
&\quad \cdot \int_{-d}^0 \mathrm{d}z' \mathrm{e}^{\kappa_\mathrm{e} z' \sec \theta} \mathbf{P}(\theta, \phi; \theta', \phi') \cdot \boldsymbol{I}(\theta', \phi', z') \Bigg], \quad (13) \\
\boldsymbol{I}(\pi - \theta, \phi, z) &= \mathrm{e}^{\kappa_\mathrm{e} z \sec \theta} \mathbf{F}(\theta) \cdot \mathbf{T}_{01}(\theta_0) \cdot \boldsymbol{I}_{0\mathrm{i}}(\pi - \theta_0, \phi_0, 0) \\
&\quad + \sec \theta \mathrm{e}^{\kappa_\mathrm{e} z \sec \theta} \frac{\kappa_\mathrm{s}}{4\pi} \int_0^\pi \sin \theta' \mathrm{d}\theta' \int_0^{2\pi} \mathrm{d}\phi' \\
&\quad \cdot \Bigg[\int_z^0 \mathrm{e}^{-\kappa_\mathrm{e} z' \sec \theta} \mathrm{d}z' \mathbf{P}(\pi - \theta, \phi; \theta', \phi') \cdot \boldsymbol{I}(\theta', \phi', z') \\
&\quad + \mathbf{F}(\theta) \cdot \mathbf{R}_{10}(\theta) \int_{-d}^0 \mathrm{e}^{\kappa_\mathrm{e} z' \sec \theta} \mathrm{d}z' \\
&\quad \cdot \mathbf{P}(\theta, \phi; \theta', \phi') \cdot \boldsymbol{I}(\theta', \phi', z') \\
&\quad + \mathbf{F}(\theta) \cdot \mathbf{R}_{10}(\theta) \cdot \mathbf{R}_{12}(\theta) \mathrm{e}^{-2\kappa_\mathrm{e} d \sec \theta} \int_{-d}^0 \mathrm{e}^{-\kappa_\mathrm{e} z' \sec \theta} \mathrm{d}z' \\
&\quad \cdot \mathbf{P}(\pi - \theta, \phi; \theta', \phi') \cdot \boldsymbol{I}(\theta', \phi', z') \Bigg], \quad (14) \\
\mathbf{F}(\theta) &= [1 - \mathbf{R}_{10}(\theta) \cdot \mathbf{R}_{12}(\theta) \exp(-2\kappa_\mathrm{e} d \sec \theta)]^{-1}. \quad (15)
\end{aligned}
$$

The first terms in (13) and (14) are the zeroth order solution. The first order solutions are obtained by substituting the zeroth order solution into the $\boldsymbol{I}(\theta', \phi', z')$ in (13) and (14) and integrating them with respect to z', θ' and ϕ'. The results are, for $0 \le \theta \le \pi/2$,

$$
\begin{aligned}
\boldsymbol{I}^{(1)}(\theta, \phi, z) &= \frac{\kappa_\mathrm{s}}{4\pi} \mathrm{e}^{-\kappa_\mathrm{e} z \sec \theta} \sec \theta \frac{\varepsilon_0 \cos \theta_{0\mathrm{i}}}{\mathrm{Re}[\varepsilon_\mathrm{eff} \varepsilon_0] \cos \theta_\mathrm{i}} \\
&\quad \cdot \Bigg\{ \mathbf{P}(\theta, \phi; \theta_\mathrm{i}, \phi_0) \cdot \boldsymbol{J}_\mathrm{u}(\theta_\mathrm{i}) \frac{1}{\kappa_\mathrm{e}(\sec \theta - \sec \theta_\mathrm{i})}
\end{aligned}
$$

$$\cdot \left[\mathrm{e}^{\kappa_\mathrm{e} z (\sec\theta - \sec\theta_\mathrm{i})} - \mathrm{e}^{-\kappa_\mathrm{e} d(\sec\theta - \sec\theta_\mathrm{i})} \right]$$

$$+ \mathbf{P}(\theta, \phi; \pi - \theta_\mathrm{i}, \phi_0) \cdot \boldsymbol{J}_\mathrm{d}(\theta_\mathrm{i}) \frac{1}{\kappa_\mathrm{e}(\sec\theta + \sec\theta_\mathrm{i})}$$

$$\cdot \left[\mathrm{e}^{\kappa_\mathrm{e} z (\sec\theta + \sec\theta_\mathrm{i})} - \mathrm{e}^{-\kappa_\mathrm{e} d(\sec\theta + \sec\theta_\mathrm{i})} \right]$$

$$+ \mathbf{F}(\theta) \cdot \mathbf{R}_{12}(\theta) \mathrm{e}^{-2\kappa_\mathrm{e} d \sec\theta}$$

$$\cdot [\mathbf{P}(\pi - \theta, \phi; \theta_\mathrm{i}, \phi_0) \cdot \boldsymbol{J}_\mathrm{u}(\theta_\mathrm{i}) D_3(\theta, \theta_\mathrm{i})$$

$$+ \mathbf{P}(\pi - \theta, \phi; \pi - \theta_\mathrm{i}, \phi_0) \cdot \boldsymbol{J}_\mathrm{d}(\theta_\mathrm{i}) D_4(\theta, \theta_\mathrm{i})]$$

$$+ \mathbf{F}(\theta) \cdot \mathbf{R}_{12}(\theta) \cdot \mathbf{R}_{10}(\theta) \mathrm{e}^{-2\kappa_\mathrm{e} d \sec\theta}$$

$$\cdot [\mathbf{P}(\theta, \phi; \theta_\mathrm{i}, \phi_0) \cdot \boldsymbol{J}_\mathrm{u}(\theta_\mathrm{i}) D_1(\theta, \theta_\mathrm{i})$$

$$\left. + \mathbf{P}(\theta, \phi; \pi - \theta_\mathrm{i}, \phi_0) \cdot \boldsymbol{J}_\mathrm{d}(\theta_\mathrm{i}) D_2(\theta, \theta_\mathrm{i})] \right\}, \qquad (16)$$

$$\boldsymbol{I}^{(1)}(\pi - \theta, \phi, z) = \frac{\kappa_\mathrm{s}}{4\pi} \mathrm{e}^{\kappa_\mathrm{e} z \sec\theta} \sec\theta \frac{\varepsilon_0 \cos\theta_{0\mathrm{i}}}{\mathrm{Re}[\varepsilon_\mathrm{eff}\varepsilon_0]\cos\theta_\mathrm{i}}$$

$$\cdot \left\{ \mathbf{P}(\pi - \theta, \phi; \theta_\mathrm{i}, \phi_0) \cdot \boldsymbol{J}_\mathrm{u}(\theta_\mathrm{i}) \frac{-1}{\kappa_\mathrm{e}(\sec\theta - \sec\theta_\mathrm{i})} \right.$$

$$\cdot \left[1 - \mathrm{e}^{-\kappa_\mathrm{e} z (\sec\theta + \sec\theta_\mathrm{i})} \right]$$

$$+ \mathbf{P}(\pi - \theta, \phi; \pi - \theta_\mathrm{i}, \phi_0) \cdot \boldsymbol{J}_\mathrm{d}(\theta_\mathrm{i}) \frac{-1}{\kappa_\mathrm{e}(\sec\theta - \sec\theta_\mathrm{i})}$$

$$\cdot \left[1 - \mathrm{e}^{-\kappa_\mathrm{e} z (\sec\theta - \sec\theta_\mathrm{i})} \right]$$

$$+ \mathbf{F}(\theta) \cdot \mathbf{R}_{10}(\theta) \cdot [\mathbf{P}(\theta, \phi; \theta_\mathrm{i}, \phi_0) \cdot \boldsymbol{J}_\mathrm{u}(\theta_\mathrm{i}) D_1(\theta, \theta_\mathrm{i})$$

$$+ \mathbf{P}(\theta, \phi; \pi - \theta_\mathrm{i}, \phi_0) \cdot \boldsymbol{J}_\mathrm{d}(\theta_\mathrm{i}) D_2(\theta, \theta_\mathrm{i})]$$

$$+ \mathbf{F}(\theta) \cdot \mathbf{R}_{10}(\theta) \cdot \mathbf{R}_{12}(\theta) \mathrm{e}^{-2\kappa_\mathrm{e} d \sec\theta}$$

$$\cdot [\mathbf{P}(\pi - \theta, \phi; \theta_\mathrm{i}, \phi_0) \cdot \boldsymbol{J}_\mathrm{u}(\theta_\mathrm{i}) D_3(\theta, \theta_\mathrm{i})$$

$$\left. + \mathbf{P}(\pi - \theta, \phi; \pi - \theta_\mathrm{i}, \phi_0) \cdot \boldsymbol{J}_\mathrm{d}(\theta_\mathrm{i}) D_4(\theta, \theta_\mathrm{i})] \right\} \quad (17)$$

where the superscript of $\boldsymbol{I}$ shows the order of iteration, Re[ ] denotes "the real part of" and θ_i is the transmission angle at $z = 0$ for propagation from region 0 to 1. Here

$$\boldsymbol{J}_\mathrm{u}(\theta_\mathrm{i}) = \mathbf{F}(\theta_\mathrm{i}) \cdot \mathbf{R}_{12}(\theta_\mathrm{i}) \cdot \mathbf{T}_{01}(\theta_{0\mathrm{i}}) \cdot \boldsymbol{I}_{0\mathrm{i}}(\pi - \theta_0, \phi_0, 0) \mathrm{e}^{-2\kappa_\mathrm{e} d \sec\theta_\mathrm{i}},$$

$$\boldsymbol{J}_\mathrm{d}(\theta_\mathrm{i}) = \mathbf{F}(\theta_\mathrm{i}) \cdot \mathbf{T}_{01}(\theta_{0\mathrm{i}}) \cdot \boldsymbol{I}_{0\mathrm{i}}(\pi - \theta_0, \phi_0, 0),$$

$$(18)$$

$$D_1(\theta_1, \theta_2) = \frac{1}{\kappa_e(\sec\theta_1 - \sec\theta_2)} \left[1 - e^{-\kappa_e d(\sec\theta_1 - \sec\theta_2)} \right],$$

$$D_2(\theta_1, \theta_2) = \frac{1}{\kappa_e(\sec\theta_1 + \sec\theta_2)} \left[1 - e^{-\kappa_e d(\sec\theta_1 + \sec\theta_2)} \right],$$

$$D_3(\theta_1, \theta_2) = \frac{-1}{\kappa_e(\sec\theta_1 + \sec\theta_2)} \left[1 - e^{\kappa_e d(\sec\theta_1 + \sec\theta_2)} \right], \qquad (19)$$

$$D_4(\theta_1, \theta_2) = \frac{-1}{\kappa_e(\sec\theta_1 - \sec\theta_2)} \left[1 - e^{\kappa_e d(\sec\theta_1 - \sec\theta_2)} \right].$$

The second order solution $\boldsymbol{I}^{(2)}(\theta, \phi, z)$ is obtained by substituting the first order solution into $\boldsymbol{I}(\theta', \phi', z')$ in (13) and (14) and carrying out integration with respect to z', θ' and ϕ'. The Stokes vector $\boldsymbol{I}(\theta, \phi, z)$ for $0 \leq \theta \leq \pi$ is expressed with good accuracy as the sum of the zeroth, first and second order solutions for the small scattering case mentioned at the beginning of Subsection 2.2;

$$\boldsymbol{I}(\theta, \phi, z) \simeq \boldsymbol{I}^{(0)}(\theta, \phi, z) + \boldsymbol{I}^{(1)}(\theta, \phi, z) + \boldsymbol{I}^{(2)}(\theta, \phi, z). \qquad (20)$$

The validity of (20) can be shown by comparing with directly numerical analysis of (1). $\boldsymbol{I}^{(1)}(\theta, \phi, 0)$ is easily obtained from (16) and (17) and the expression of $\boldsymbol{I}^{(2)}(\theta, \phi, 0)$ for $0 \leq \theta \leq \pi/2$ is given in Appendix B. Then, the scattered Stokes vector and the backscattering cross section are obtained from (11) and (12), respectively.

3. NUMERICAL RESULTS

In this section, we numerically shows the scattering cross section of a moist soil model $\sigma_{\beta\alpha}$ by changing the fractional volume of water f_w and the incident angle and polarization of incident waves. We also discuss the possibility of sensing the water content of soil for the simple model by characterizing the scattering cross sections as a function of f_w. The physical parameters are assumed to be the operating frequency $\nu = 2\,\text{GHz}$, $\varepsilon_g = 3.0$ and $a = 1\,\text{mm}$, and the dielectric constant of water ε_w is calculated from Debye's equation [4]. The parameters in the DMRT are determined by using the equations (3) to (8).

3.1. Scattering from Free Water

We first assume that the particles are homogeneous spherical water drops of $\varepsilon_w \varepsilon_0$; hence we have $f_w = f$. Figure 2 shows κ_e, κ_s and ε_{eff} as functions of f_w. We can find that κ_e and ε_{eff} increase monotonically as f_w becomes large while κ_s increases until around $f_w = 0.2$ and then decreases. This behavior is physically valid and different from that of the CRT.
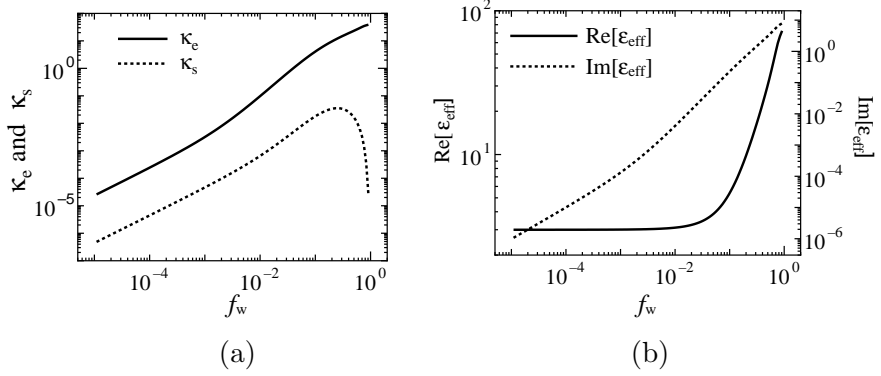
Figure 2. (a) The extinction rate κ_e, the scattering coefficient κ_s and (b) the effective dielectric constant ε_{eff} as a function of the fractional volume of water f_w, when the operating frequency is $2\,\text{GHz}$, $a = 1\,\text{mm}$, $\varepsilon_g = 3.0$.
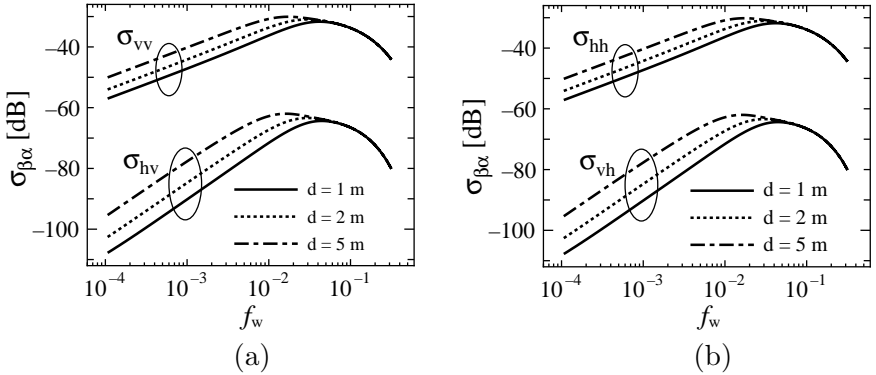

Figure 3. The backscattering cross section $\sigma_{\beta\alpha}$ as a function of the fractional volume of water f_w for both cases: (a) v-polarized wave intensity incidence and (b) h-polarized wave intensity incidence, when the operating frequency is $2\,\text{GHz}$, $a = 1\,\text{mm}$, $\varepsilon_g = 3.0$, $\varepsilon_2 = \varepsilon_{eff}$, $d = 1,\ 2,\ 5\,\text{m}$, $\theta_{0i} = 13.7$ degree.

We consider effects of the layer thickness on $\sigma_{\beta\alpha}$. Figure 3 shows $\sigma_{\beta\alpha}$ as a function of f_w for $\theta_{0i} = 13.7$ degree, $\varepsilon_2 = \varepsilon_{eff}$ and $d = 1,\ 2$ and $5\,\text{m}$. The $\sigma_{\beta\alpha}$ behaves as a convex function of f_w for the three cases of d. As f_w becomes larger than about 0.05, all the $\sigma_{\beta\alpha}$ have the same value, which means that $\sigma_{\beta\alpha}$ does not depend on the layer thickness for the case of $d \geq 1$ m. The smaller d makes larger the value of f_w at which $\sigma_{\beta\alpha}$ takes a maximum.
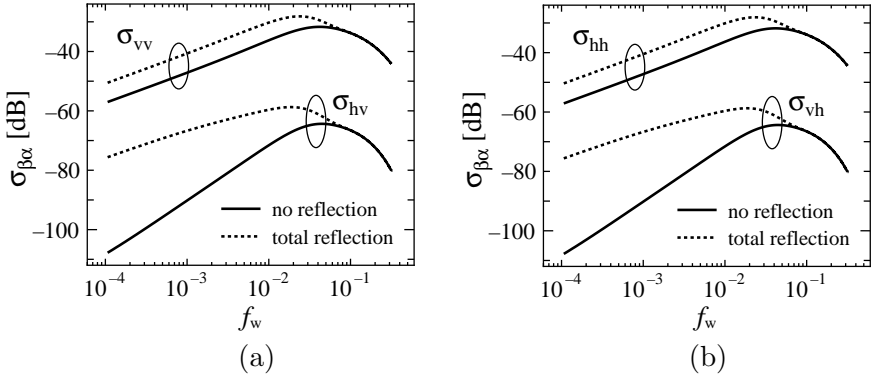
Figure 4. As Fig. 3, but with $\varepsilon_2 = \varepsilon_{\text{eff}}, \infty$ and $d = 1\,\text{m}$.

Next we assume $\varepsilon_2 = \varepsilon_{\text{eff}}$ (no reflection) and $\varepsilon_2 = \infty$ (total reflection) to investigate the effect of bottom layer. Figure 4 depicts the effect on $\sigma_{\beta\alpha}$. For $f_{\text{w}} < 0.05$, the multi-reflection of waves due to both boundaries at $z = 0$ and $-d$ yields the increase in $\sigma_{\beta\alpha}$ for total reflection case. The bottom layer makes a small contribution to σ_{vv} and σ_{hh} compared with σ_{vh} and σ_{hv} because the co-polarized wave intensity mainly depends on the first order solution. This result suggests that σ_{vh} and σ_{hv} are applicable to the detection of the bottom layer if these cross-polarized wave intensities are measurable.

Although $\sigma_{\beta\alpha}$ depends on the layer thickness and the bottom layer for small f_{w}, it has such a common property that it first increases to a certain level and then decreases as f_{w} becomes large. Therefore we have one value of $\sigma_{\beta\alpha}$ at different two values of f_{w} and cannot determine f_{w} directly from the measurement of $\sigma_{\beta\alpha}$.

The ratio of σ_{vv} to σ_{hh} is illustrated in Fig. 5 for $\theta_{0\text{i}} = 13.7$, 33.7 and 53.7 degree and $\varepsilon_2 = \varepsilon_{\text{eff}}$. Figure 5 shows that $\sigma_{\text{vv}}/\sigma_{\text{hh}}$ is more sensitive to larger incident angles. The trade-off for the large change in $\sigma_{\text{vv}}/\sigma_{\text{hh}}$ is the decrease in $\sigma_{\alpha\alpha}$ for large incident angles. Figure 6 shows $\sigma_{\text{vv}}/\sigma_{\text{hh}}$ as a function of f_{w} when $d = 1$, 2 and $5\,\text{m}$, $\varepsilon_2 = \varepsilon_{\text{eff}}$ and ∞ and $\theta_{0\text{i}} = 53.7$ degree. We can observe that the difference of $\sigma_{\text{vv}}/\sigma_{\text{hh}}$ between no and total reflection cases is about $4\,\text{dB}$ at $f_{\text{w}} < 0.001$, independent of the layer thickness and that there is a one-to-one correspondence between $\sigma_{\text{vv}}/\sigma_{\text{hh}}$ and f_{w} at $f_{\text{w}} > 0.05$. The one-to-one correspondence means that the measurement of $\sigma_{\text{vv}}/\sigma_{\text{hh}}$ is applicable to sensing of the soil moisture at $f_{\text{w}} > 0.05$. The threshold value of f_{w}, at which $\sigma_{\text{vv}}/\sigma_{\text{hh}}$ becomes independent of the bottom layer, becomes small for large d.
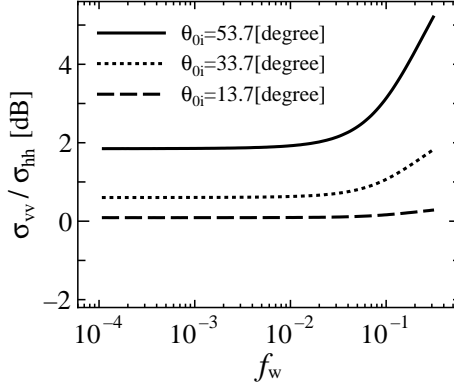
Figure 5. The ratio of σ_{vv} to σ_{hh} as a function of the fractional volume of water f_w, when the operating frequency $= 2\,\text{GHz}$, $a = 1\,\text{mm}$, $\varepsilon_g = 3.0$, $\varepsilon_2 = \varepsilon_{\text{eff}}$, $d = 1\,\text{m}$, $\theta_{0i} = 13.7$, 33.7, 53.7 degree.

3.2. Scattering from Soil Particles Coated with Water

It is well known that bound water, which coats soil particle, mainly contributes to the dielectric properties of moist soil. Therefore, in this subsection we assume particles of radius a to be spherical soil particles of $\varepsilon_s \varepsilon_0$ and radius a_1 coated with water, as shown in Fig. 7. In this case, $f_w = (1 - a_1^3/a^3)f$, and we assume $\varepsilon_s = 4.7$ [4]. The ratio of a_1 to a is assumed to be 0.9, 0.75, 0.5, and 0.0, where particles of $a_1/a = 0.0$ correspond to free water drops. In the following calculations, the value of f is considered to be up to 0.63 because spheres are deformed at $f > 0.63$; hence the maximum values of f_w for $a_1/a = 0.9$, 0.75, 0.5, and 0.0 are 0.17, 0.36, 0.55, and 0.63, respectively.

   We clarify the effects of coating water on $\sigma_{\beta\alpha}$ and σ_{vv}/σ_{hh}. The σ_{vv} and σ_{hv} for no and total reflection case are illustrated in Figs. 8 and 9, respectively, by assuming the same physical parameters as used in Fig. 3, but $\theta_{0i} = 53.7$ degree. The σ_{hh} and σ_{vh} also are depicted in Figs. 10 and 11 under the same physical conditions of the model as used in Figs. 8 and 9, respectively. These figures 8 to 11 show that all the $\sigma_{\beta\alpha}$ have the peak values at smaller f_w as a_1/a increases. We can observe that the thickness of coating water has large contribution to the $\sigma_{\beta\alpha}$. These behaviors of $\sigma_{\beta\alpha}$ are explained from the following facts. The $\sigma_{\beta\alpha}$ have the similar curves as a function of f for all the a_1/a except for their magnitude. The value of f at a certain value of f_w depend on a_1/a because of $f_w = (1 - a_1^3/a^3)f$. Therefore $\sigma_{\beta\alpha}$ show different curves as a function of f_w for all the a_1/a. Figure 12 shows σ_{vv}/σ_{hh} as a function of f_w for $\theta_{0i} = 53.7$ degree. This figure indicates
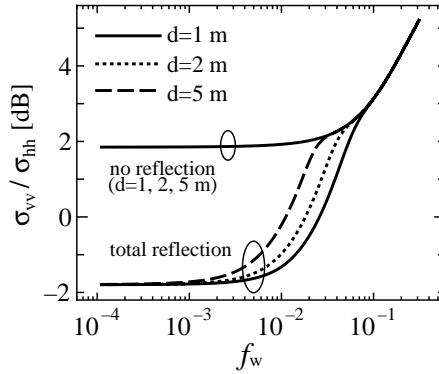
Figure 6. As Fig. 5, but with $\varepsilon_2 = \varepsilon_{\text{eff}}, \infty$, $d = 1, 2, 5\,\text{m}$ and $\theta_{0i} = 53.7$ degree.
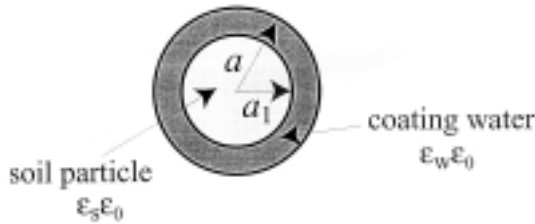
Figure 7. Soil particle coated with water.
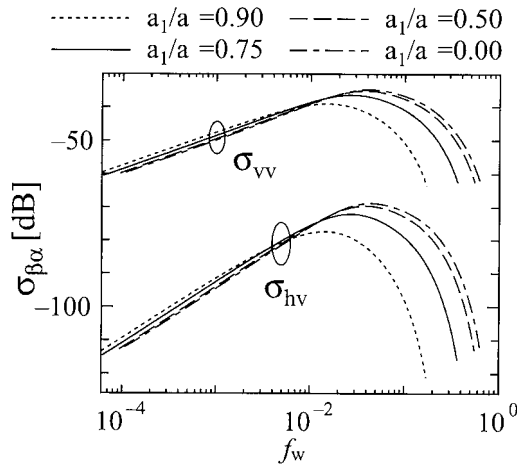
Figure 8. The backscattering cross section $\sigma_{\beta\alpha}$ as a function of the fractional volume of water f_w, when the operating frequency $= 2\,\text{GHz}$, $a = 1\,\text{mm}$, $\varepsilon_g = 3.0$, $\varepsilon_s = 4.7$, $\varepsilon_2 = \varepsilon_{\text{eff}}$, $d = 1\,\text{m}$, $\theta_{0i} = 53.7$ degree.

Figure 9. As Fig. 8, but with $\varepsilon_2 = \infty$.

Figure 10. As Fig. 8, but with h-polarized wave intensity incidence.

Figure 11. As Fig. 9, but with h-polarized wave intensity incidence.
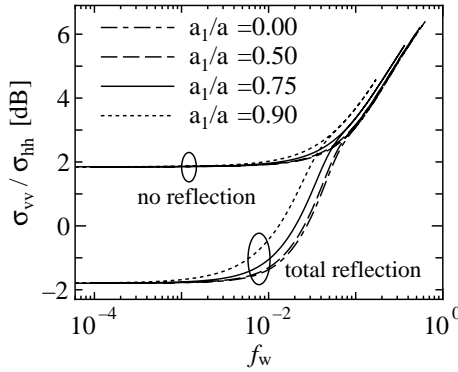
Figure 12. The ratio of σ_{vv} to σ_{hh} as a function of the fractional volume of water f_{w}, when the operating frequency=2 GHz, a= 1 mm, $\varepsilon_{\mathrm{g}} = 3.0$, $\varepsilon_2 = \varepsilon_{\mathrm{eff}}$, $d = 1$ m, $\theta_{0\mathrm{i}} = 53.7$ degree, $a_1/a = 0.9, 0.75, 0.5, 0.0$.

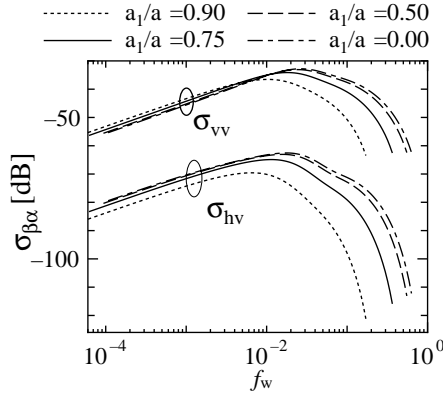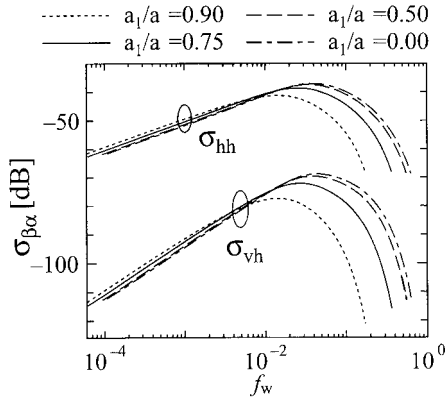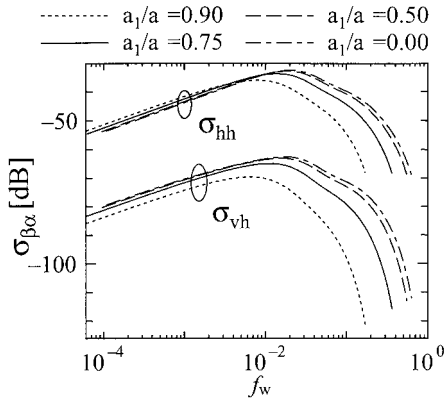that the difference of the thickness of coating water contributes much less to $\sigma_{\mathrm{vv}}/\sigma_{\mathrm{hh}}$ than $\sigma_{\beta\alpha}$ for large f_{w}, because the thickness effects on σ_{vv} and σ_{hh} are almost the same.

4. CONCLUSION

We have assumed a moist soil model as a random medium layer sandwiched between free space and a homogeneous bottom space and evaluated scattering cross sections of the layer by using a dense medium radiative transfer equation (DMRT). A multiple scattering method applicable to a random medium containing many particles of high dielectric constant has been used to estimate the parameters in the DMRT. We have clarified the characteristics of scattering cross sections of the layer by changing the incident angle and polarization of incident waves and the water content. We have also computed the scattering cross sections for two types of spherical particles: free water and soil particles coated with water. The detection possibility of a water content of soil has been discussed mainly on the basis of the following characteristics. One is that the ratio of the co-polarized backscattering cross section for vertical polarization incidence to that for horizontal polarization incidence has an one-to-one correspondence to a volumetric water content larger than 0.05. The other is that the ratio is less dependent on the thickness of coating water than the scattering cross sections of the layer are.

ACKNOWLEGMENT

APPENDIX A. BOUNDARY CONDITIONS FOR THE STOKES VECTOR AT A PLANE SURFACE

When a plane-wave is incident on a medium of ε_j from one of ε_i with incident angle θ_i, the reflection and transmission matrices at the plane surface $\mathbf{R}_{\mathrm{ij}}(\theta_\mathrm{i})$ and $\mathbf{T}_{\mathrm{ij}}(\theta_\mathrm{i})$ are given as follows:

$$
\mathbf{R}_{\mathrm{ij}}(\theta_\mathrm{i}) = \begin{bmatrix} r_{\mathrm{ij}}^{\mathrm{v}}(\theta_\mathrm{i}) & 0 & 0 & 0 \\ 0 & r_{\mathrm{ij}}^{\mathrm{h}}(\theta_\mathrm{i}) & 0 & 0 \\ 0 & 0 & \mathrm{Re}[R_{\mathrm{ij}}^{\mathrm{h}}(\theta_\mathrm{i})R_{\mathrm{ij}}^{\mathrm{v}*}(\theta_\mathrm{i})] & -\mathrm{Im}[R_{\mathrm{ij}}^{\mathrm{h}}(\theta_\mathrm{i})R_{\mathrm{ij}}^{\mathrm{v}*}(\theta_\mathrm{i})] \\ 0 & 0 & \mathrm{Im}[R_{\mathrm{ij}}^{\mathrm{h}}(\theta_\mathrm{i})R_{\mathrm{ij}}^{\mathrm{v}*}(\theta_\mathrm{i})] & \mathrm{Re}[R_{\mathrm{ij}}^{\mathrm{h}}(\theta_\mathrm{i})R_{\mathrm{ij}}^{\mathrm{v}*}(\theta_\mathrm{i})] \end{bmatrix}
$$
(A1)

and

$$
\mathbf{T}_{\mathrm{ij}}(\theta_\mathrm{i}) = \frac{\varepsilon_\mathrm{j}}{\varepsilon_\mathrm{i}} \begin{bmatrix} t_{\mathrm{ij}}^{\mathrm{v}}(\theta_\mathrm{i}) & 0 & 0 \\ 0 & t_{\mathrm{ij}}^{\mathrm{h}}(\theta_\mathrm{i}) & 0 \\ 0 & 0 & \dfrac{\cos\theta_\mathrm{t}}{\cos\theta_\mathrm{i}}\mathrm{Re}[T_{\mathrm{ij}}^{\mathrm{h}}(\theta_\mathrm{i})T_{\mathrm{ij}}^{\mathrm{v}*}(\theta_\mathrm{i})] \\ 0 & 0 & \dfrac{\cos\theta_\mathrm{t}}{\cos\theta_\mathrm{i}}\mathrm{Im}[T_{\mathrm{ij}}^{\mathrm{h}}(\theta_\mathrm{i})T_{\mathrm{ij}}^{\mathrm{v}*}(\theta_\mathrm{i})] \end{bmatrix.
$$

$$
\left. \begin{matrix} 0 \\ 0 \\ -\dfrac{\cos\theta_\mathrm{t}}{\cos\theta_\mathrm{i}}\mathrm{Im}[T_{\mathrm{ij}}^{\mathrm{h}}(\theta_\mathrm{i})T_{\mathrm{ij}}^{\mathrm{v}*}(\theta_\mathrm{i})] \\ \dfrac{\cos\theta_\mathrm{t}}{\cos\theta_\mathrm{i}}\mathrm{Re}[T_{\mathrm{ij}}^{\mathrm{h}}(\theta_\mathrm{i})T_{\mathrm{ij}}^{\mathrm{v}*}(\theta_\mathrm{i})] \end{matrix} \right]
$$
(A2)

where, $R(T)_{\mathrm{ij}}^{\mathrm{h}}, R(T)_{\mathrm{ij}}^{\mathrm{v}}$ denote the Fresnel reflection (transmission) coefficients of h and v polarized waves, respectively. The asterisk denotes complex conjugate, θ_t is the transmission angle, and

$$
\begin{align}
T_{\mathrm{ij}}^{\mathrm{v}}(\theta_\mathrm{i}) &= 1 + R_{\mathrm{ij}}^{\mathrm{v}}(\theta_\mathrm{i}) \tag{A3} \\
T_{\mathrm{ij}}^{\mathrm{h}}(\theta_\mathrm{i}) &= 1 + R_{\mathrm{ij}}^{\mathrm{h}}(\theta_\mathrm{i}) \tag{A4} \\
r_{\mathrm{ij}}^{\mathrm{v}}(\theta_\mathrm{i}) &= |R_{\mathrm{ij}}^{\mathrm{v}}(\theta_\mathrm{i})|^2 \tag{A5} \\
r_{\mathrm{ij}}^{\mathrm{h}}(\theta_\mathrm{i}) &= |R_{\mathrm{ij}}^{\mathrm{h}}(\theta_\mathrm{i})|^2 \tag{A6} \\
t_{\mathrm{ij}}^{\mathrm{v}}(\theta_\mathrm{i}) &= 1 - r_{\mathrm{ij}}^{\mathrm{v}}(\theta_\mathrm{i}) \tag{A7} \\
t_{\mathrm{ij}}^{\mathrm{h}}(\theta_\mathrm{i}) &= 1 - r_{\mathrm{ij}}^{\mathrm{h}}(\theta_\mathrm{i}). \tag{A8}
\end{align}
$$

APPENDIX B. SECOND ORDER SOLUTION $\boldsymbol{I}^{(2)}(\theta, \phi, 0)$ FOR $0 \leq \theta \leq \pi/2$

$$\boldsymbol{I}^{(2)}(\theta, \phi, 0) = \sec\theta \mathbf{F}(\theta) \cdot \int_0^{\pi/2} \mathrm{d}\theta' \sin\theta' \sec\theta' \frac{\varepsilon_0 \cos\theta_{0\mathrm{i}}}{\mathrm{Re}[\varepsilon_{\mathrm{eff}}\varepsilon_0]\cos\theta_{\mathrm{i}}}$$

$$\cdot \left\{ \mathbf{M}(\theta, \theta'; \mathbf{E}; \theta', \theta_{\mathrm{i}}) \cdot \boldsymbol{J}_{\mathrm{u}}(\theta_{\mathrm{i}}) \frac{1}{\kappa_{\mathrm{e}}(\sec\theta' - \sec\theta_{\mathrm{i}})} \right.$$

$$\cdot \left[D_1(\theta, \theta_{\mathrm{i}}) - D_1(\theta, \theta')\mathrm{e}^{-\kappa_{\mathrm{e}}d(\sec\theta' - \sec\theta_{\mathrm{i}})} \right]$$

$$+ \mathbf{M}(\theta, \theta'; \mathbf{E}; \theta', \pi - \theta_{\mathrm{i}}) \cdot \boldsymbol{J}_{\mathrm{d}}(\theta_{\mathrm{i}}) \frac{1}{\kappa_{\mathrm{e}}(\sec\theta' + \sec\theta_{\mathrm{i}})}$$

$$\cdot \left[D_2(\theta, \theta_{\mathrm{i}}) - D_1(\theta, \theta')\mathrm{e}^{-\kappa_{\mathrm{e}}d(\sec\theta' + \sec\theta_{\mathrm{i}})} \right] + \mathrm{e}^{-2\kappa_{\mathrm{e}}d\sec\theta'}$$

$$\cdot \left[\mathbf{M}(\theta, \theta'; \mathbf{F}\mathbf{R}_{12}; \pi - \theta', \theta_{\mathrm{i}}) \cdot \boldsymbol{J}_{\mathrm{u}}(\theta_{\mathrm{i}}) D_3(\theta', \theta_{\mathrm{i}}) \right.$$

$$+ \mathbf{M}(\theta, \theta'; \mathbf{F}\mathbf{R}_{12}; \pi - \theta', \pi - \theta_{\mathrm{i}}) \cdot \boldsymbol{J}_{\mathrm{d}}(\theta_{\mathrm{i}}) D_4(\theta', \theta_{\mathrm{i}}) \big] \, D_1(\theta, \theta')$$

$$+ \mathrm{e}^{-2\kappa_{\mathrm{e}}d\sec\theta'} \big[\mathbf{M}(\theta, \theta'; \mathbf{F}\mathbf{R}_{12}\mathbf{R}_{10}; \theta', \theta_{\mathrm{i}}) \cdot \boldsymbol{J}_{\mathrm{u}}(\theta_{\mathrm{i}}) D_1(\theta', \theta_{\mathrm{i}})$$

$$+ \mathbf{M}(\theta, \theta'; \mathbf{F}\mathbf{R}_{12}\mathbf{R}_{10}; \theta', \pi - \theta_{\mathrm{i}}) \cdot \boldsymbol{J}_{\mathrm{d}}(\theta_{\mathrm{i}}) D_2(\theta', \theta_{\mathrm{i}}) \big] \, D_1(\theta, \theta')$$

$$+ \mathbf{M}(\theta, \pi - \theta'; \mathbf{E}; \pi - \theta', \theta_{\mathrm{i}}) \cdot \boldsymbol{J}_{\mathrm{u}}(\theta_{\mathrm{i}}) \frac{-1}{\kappa_{\mathrm{e}}(\sec\theta' + \sec\theta_{\mathrm{i}})}$$

$$\cdot \left[D_2(\theta, \theta') - D_1(\theta, \theta_{\mathrm{i}}) \right] + \mathbf{M}(\theta, \pi - \theta'; \mathbf{E}; \pi - \theta', \pi - \theta_{\mathrm{i}})$$

$$\cdot \boldsymbol{J}_{\mathrm{d}}(\theta_{\mathrm{i}}) \frac{-1}{\kappa_{\mathrm{e}}(\sec\theta' - \sec\theta_{\mathrm{i}})} \left[D_2(\theta, \theta') - D_2(\theta, \theta_{\mathrm{i}}) \right]$$

$$+ \big[\mathbf{M}(\theta, \pi - \theta'; \mathbf{F}\mathbf{R}_{10}; \theta', \theta_{\mathrm{i}}) \cdot \boldsymbol{J}_{\mathrm{u}}(\theta_{\mathrm{i}}) D_1(\theta', \theta_{\mathrm{i}})$$

$$+ \mathbf{M}(\theta, \pi - \theta'; \mathbf{F}\mathbf{R}_{10}; \theta', \pi - \theta_{\mathrm{i}}) \cdot \boldsymbol{J}_{\mathrm{d}}(\theta_{\mathrm{i}}) D_2(\theta', \theta_{\mathrm{i}}) \big] D_2(\theta, \theta')$$

$$+ \mathrm{e}^{-2\kappa_{\mathrm{e}}d\sec\theta'} \big[\mathbf{M}(\theta, \pi - \theta'; \mathbf{F}\mathbf{R}_{10}\mathbf{R}_{12}; \pi - \theta', \theta_{\mathrm{i}})$$

$$\cdot \boldsymbol{J}_{\mathrm{u}}(\theta_{\mathrm{i}}) D_3(\theta', \theta_{\mathrm{i}}) + \mathbf{M}(\theta, \pi - \theta'; \mathbf{F}\mathbf{R}_{10}\mathbf{R}_{12}; \pi - \theta', \pi - \theta_{\mathrm{i}})$$

$$\left. \cdot \boldsymbol{J}_{\mathrm{d}}(\theta_{\mathrm{i}}) D_4(\theta', \theta_{\mathrm{i}}) \big] \, D_2(\theta, \theta') \right\} + \sec\theta \mathbf{F}(\theta) \cdot \mathbf{R}_{12}(\theta)$$

$$\cdot \mathrm{e}^{-2\kappa_{\mathrm{e}}d\sec\theta} \int_0^{\pi/2} \mathrm{d}\theta' \sin\theta' \sec\theta' \frac{\varepsilon_0 \cos\theta_{0\mathrm{i}}}{\mathrm{Re}[\varepsilon_{\mathrm{eff}}\varepsilon_0]\cos\theta_{\mathrm{i}}}$$

$$\cdot \left\{ \mathbf{M}(\pi - \theta, \theta'; \mathbf{E}; \theta', \theta_{\mathrm{i}}) \cdot \boldsymbol{J}_{\mathrm{u}}(\theta_{\mathrm{i}}) \frac{1}{\kappa_{\mathrm{e}}(\sec\theta' - \sec\theta_{\mathrm{i}})} \right.$$

$$\cdot \left[D_3(\theta, \theta_{\mathrm{i}}) - D_3(\theta, \theta')\mathrm{e}^{-\kappa_{\mathrm{e}}d(\sec\theta' - \sec\theta_{\mathrm{i}})} \right]$$

$$+ \mathbf{M}(\pi - \theta, \theta'; \mathbf{E}; \theta', \pi - \theta_{\mathrm{i}}) \cdot \boldsymbol{J}_{\mathrm{d}}(\theta_{\mathrm{i}}) \frac{1}{\kappa_{\mathrm{e}}(\sec\theta' + \sec\theta_{\mathrm{i}})}$$

$$\cdot \left[D_4(\theta, \theta_{\mathrm{i}}) - D_3(\theta, \theta') \mathrm{e}^{-\kappa_{\mathrm{e}} d (\sec \theta' + \sec \theta_{\mathrm{i}})} \right]$$

$$+ \mathrm{e}^{-2\kappa_{\mathrm{e}} d \sec \theta'} \left[\mathbf{M}(\pi - \theta, \theta'; \mathbf{FR}_{12}; \pi - \theta', \theta_{\mathrm{i}}) \right.$$

$$\cdot \boldsymbol{J}_{\mathrm{u}}(\theta_{\mathrm{i}}) D_3(\theta', \theta_{\mathrm{i}}) + \mathbf{M}(\pi - \theta, \theta'; \mathbf{FR}_{12}; \pi - \theta', \pi - \theta_{\mathrm{i}})$$

$$\cdot \boldsymbol{J}_{\mathrm{d}}(\theta_{\mathrm{i}}) D_4(\theta', \theta_{\mathrm{i}}) \left] D_3(\theta, \theta') + \mathrm{e}^{-2\kappa_{\mathrm{e}} d \sec \theta'} \right.$$

$$\cdot \left[\mathbf{M}(\pi - \theta, \theta'; \mathbf{FR}_{12}\mathbf{R}_{10}; \theta', \theta_{\mathrm{i}}) \cdot \boldsymbol{J}_{\mathrm{u}}(\theta_{\mathrm{i}}) D_1(\theta', \theta_{\mathrm{i}}) \right.$$

$$+ \mathbf{M}(\pi - \theta, \theta'; \mathbf{FR}_{12}\mathbf{R}_{10}; \theta', \pi - \theta_{\mathrm{i}}) \cdot \boldsymbol{J}_{\mathrm{d}}(\theta_{\mathrm{i}}) D_2(\theta', \theta_{\mathrm{i}})] D_3(\theta, \theta')$$

$$+ \mathbf{M}(\pi - \theta, \pi - \theta'; \mathbf{E}; \pi - \theta', \theta_{\mathrm{i}}) \cdot \boldsymbol{J}_{\mathrm{u}}(\theta_{\mathrm{i}}) \frac{-1}{\kappa_{\mathrm{e}}(\sec \theta' + \sec \theta_{\mathrm{i}})}$$

$$\cdot \left[D_4(\theta, \theta') - D_3(\theta, \theta_{\mathrm{i}}) \right] + \mathbf{M}(\pi - \theta, \pi - \theta'; \mathbf{E}; \pi - \theta', \pi - \theta_{\mathrm{i}})$$

$$\cdot \boldsymbol{J}_{\mathrm{d}}(\theta_{\mathrm{i}}) \frac{-1}{\kappa_{\mathrm{e}}(\sec \theta' - \sec \theta_{\mathrm{i}})} \left[D_4(\theta, \theta') - D_4(\theta, \theta_{\mathrm{i}}) \right]$$

$$+ \left[\mathbf{M}(\pi - \theta, \pi - \theta'; \mathbf{FR}_{10}; \theta', \theta_{\mathrm{i}}) \cdot \boldsymbol{J}_{\mathrm{u}}(\theta_{\mathrm{i}}) D_1(\theta', \theta_{\mathrm{i}}) \right.$$

$$+ \mathbf{M}(\pi - \theta, \pi - \theta'; \mathbf{FR}_{10}; \theta', \pi - \theta_{\mathrm{i}}) \cdot \boldsymbol{J}_{\mathrm{d}}(\theta_{\mathrm{i}}) D_2(\theta', \theta_{\mathrm{i}})]$$

$$\cdot D_4(\theta, \theta') + \mathrm{e}^{-2\kappa_{\mathrm{e}} d \sec \theta'} \left[\mathbf{M}(\pi - \theta, \pi - \theta'; \mathbf{FR}_{10}\mathbf{R}_{12}; \pi - \theta', \theta_{\mathrm{i}}) \right.$$

$$\cdot \boldsymbol{J}_{\mathrm{u}}(\theta_{\mathrm{i}}) D_3(\theta', \theta_{\mathrm{i}}) + \mathbf{M}(\pi - \theta, \pi - \theta'; \mathbf{FR}_{10}\mathbf{R}_{12};$$

$$\pi - \theta', \pi - \theta_{\mathrm{i}}) \cdot \boldsymbol{J}_{\mathrm{d}}(\theta_{\mathrm{i}}) D_4(\theta', \theta_{\mathrm{i}}) \left] D_4(\theta, \theta') \right\} \tag{B1}$$

where $\mathbf{E}$ denotes the unit matrix and

$$\mathbf{M}(\theta, \theta_1; \mathbf{AB}; \theta_2, \theta_{\mathrm{i}}) = \left(\frac{\kappa_{\mathrm{s}}}{4\pi} \right)^2 \int_0^{2\pi} \mathbf{P}(\theta, \phi; \theta_1, \phi')$$
$$\cdot \mathbf{A}(\theta_2) \cdot \mathbf{B}(\theta_2) \cdot \mathbf{P}(\theta_2, \phi'; \theta_{\mathrm{i}}, \phi_{\mathrm{i}}) \mathrm{d}\phi'. \tag{B2}$$

REFERENCES

1. Dobson, M. C. and F. T. Ulaby, "Active microwave soil moisture research," *IEEE Trans. Geosci. & Remote Sens.,* Vol. 24, 23–36, 1986.

2. Schmugge, T., P. E. O'Neill, and J. R. Wang, "Passive microwave soil moisture research," *IEEE Trans. Geosci. & Remote Sens.,* Vol. 24, 12–22, 1986.

3. Wang, J. R. and T. J. Schmugge, "An empirical model for the complex dielectric permittivity of soils as a function of water content," *IEEE Trans. Geosci. & Remote Sens.,* Vol. 18, 288–295, 1980.

4. Ulaby, F. T., R. K. Moore, and A. K. Fung, *Microwave Remote Sensing,* Vol. 3, Artech House, Dedham, MA, 1986.

5. Tateiba, M., Y. Nanbu, and T. Oe, "Numerical analysis of the effective dielectric constant of the medium where dielectric spheres are randomly distributed," *IEICE Trans. Electron.,* Vol. E76-C, 1461–1467, 1993.

6. Nanbu, Y. and M. Tateiba, "Comparative study of the effective dielectric constant of a medium containing randomly distributed dielectric spheres embedded in a homogeneous background medium," *Waves in Random Media,* Vol. 6, 347–360, 1996.

7. Tsang, L. and A. Ishimaru, "Radiative wave equations for vector electromagnetic propagation in dense nontenuous media," *J. Electromagn. Waves & Appl.,* Vol. 1, 59–72, 1987.

8. Tateiba, M., "A new approach to the problem of wave scattering by many particles," *Radio Sci.,* Vol. 22, 881–884, 1987.

9. Tateiba, M., "Electromagnetic wave scattering in media whose particles are randomly displaced from a uniformly ordered spatial distribution," *IEICE Trans. Electron.,* Vol. E78-C, 1357–1365, 1995.

10. Matsuoka, T. and M. Tateiba, "Comparison of scattered power from a layer with randomly distributed lossy spheres of high dielectric constant by using radiative transfer theory," *IEICE Trans. Electron.,* Vol. E83-C, No. 12, 1803–1808, 2000.

11. Tsang, L. and A. Ishimaru, "Theory of backscattering enhancement of random discrete isotropic scatterers based on the summation of all ladder and cyclical terms," *Journal of Optical Society of America,* A, Vol. 2, 1331–1338, 1985.

12. Chandrasekhar, S., *Radiative Transfer,* Dover, New York, 1960.

13. Shin, R. T. and J. A. Kong, "Radiative transfer theory for active remote sensing of a homogeneous layer containing spherical scatterers," *Journal of Applied Physics,* Vol. 52, 4221–4230, 1981.

14. Ulaby, F. T., P. P. Batlivala, and M. C. Dobson, "Microwave backscatter dependence on surface roughness, soil moisture, and soil texture: Part I – bare soil," *IEEE Trans. Geosci. & Electron.,* Vol. 16, 286–295, 1978.

15. Schmugge, T. J., "Remote sensing of soil moisture: Recent advances," *IEEE Trans. Geosci. & Remote Sens.,* Vol. 21, 336–344, 1983.

16. Tsang, L. and J. A. Kong, "Radiative transfer theory for active remote sensing of half – space random media," *Radio Sci.,* Vol. 13, 763–773, 1978.

17. Barabanenkov, Y. N, "On the spectral theory of radiation transport equations," *Sov. Phys.–JETP,* Vol. 29, 679–684, 1969.

18. Tsang, L., J. A. Kong, and R. T. Shin, *Theory of Microwave Remote Sensing,* Wiley Interscience, New York, 1985.

19. Ishimaru, A., *Wave Propagation and Scattering in Random Media,* IEEE Press, Piscataway NJ, 1997.